



Radiative forcing by well-mixed greenhouse gases: Estimates from climate models in the Intergovernmental Panel on Climate Change (IPCC) Fourth Assessment Report (AR4)

W. D. Collins,¹ V. Ramaswamy,² M. D. Schwarzkopf,² Y. Sun,³ R. W. Portmann,⁴
Q. Fu,⁵ S. E. B. Casanova,⁶ J.-L. Dufresne,⁷ D. W. Fillmore,⁸ P. M. D. Forster,⁹
V. Y. Galin,¹⁰ L. K. Gohar,⁶ W. J. Ingram,¹¹ D. P. Kratz,¹² M.-P. Lefebvre,⁷ J. Li,¹³
P. Marquet,¹⁴ V. Oinas,¹⁵ Y. Tsushima,¹⁶ T. Uchiyama,¹⁷ and W. Y. Zhong¹⁸

Received 26 September 2005; revised 11 February 2006; accepted 7 April 2006; published 28 July 2006.

[1] The radiative effects from increased concentrations of well-mixed greenhouse gases (WMOGHGs) represent the most significant and best understood anthropogenic forcing of the climate system. The most comprehensive tools for simulating past and future climates influenced by WMOGHGs are fully coupled atmosphere-ocean general circulation models (AOGCMs). Because of the importance of WMOGHGs as forcing agents it is essential that AOGCMs compute the radiative forcing by these gases as accurately as possible. We present the results of a radiative transfer model intercomparison between the forcings computed by the radiative parameterizations of AOGCMs and by benchmark line-by-line (LBL) codes. The comparison is focused on forcing by CO₂, CH₄, N₂O, CFC-11, CFC-12, and the increased H₂O expected in warmer climates. The models included in the intercomparison include several LBL codes and most of the global models submitted to the Intergovernmental Panel on Climate Change (IPCC) Fourth Assessment Report (AR4). In general, the LBL models are in excellent agreement with each other. However, in many cases, there are substantial discrepancies among the AOGCMs and between the AOGCMs and LBL codes. In some cases this is because the AOGCMs neglect particular absorbers, in particular the near-infrared effects of CH₄ and N₂O, while in others it is due to the methods for modeling the radiative processes. The biases in the AOGCM forcings are generally largest at the surface level. We quantify these differences and discuss the implications for interpreting variations in forcing and response across the multimodel ensemble of AOGCM simulations assembled for the IPCC AR4.

Citation: Collins, W. D., et al., (2006), Radiative forcing by well-mixed greenhouse gases: Estimates from climate models in the Intergovernmental Panel on Climate Change (IPCC) Fourth Assessment Report (AR4), *J. Geophys. Res.*, *111*, D14317, doi:10.1029/2005JD006713.

1. Introduction

[2] One of the major factors underlying recent climate change is radiative forcing. Radiative forcing is an externally imposed change in the radiative energy budget of the

Earth's climate system [*Intergovernmental Panel on Climate Change (IPCC)*, 2001]. The energy budget is characterized by an approximate balance between shortwave absorption and longwave emission by the climate system [e.g., *Kiehl*

¹National Center for Atmospheric Research, Boulder, Colorado, USA.

²Geophysical Fluid Dynamics Laboratory, Princeton, New Jersey, USA.

³National Climate Center, Beijing, China.

⁴Aeronomy Laboratory, NOAA, Boulder, Colorado, USA.

⁵Department of Atmospheric Sciences, University of Washington, Seattle, Washington, USA.

⁶Department of Meteorology, University of Reading, Reading, UK.

⁷Laboratoire de Météorologie Dynamique, Paris, France.

⁸Le Laboratoire des Sciences du Climat et l'Environnement, Gif-sur-Yvette, France.

⁹School of Earth and Environment, University of Leeds, Leeds, UK.

¹⁰Institute of Numerical Mathematics, Academy of Sciences, Moscow, Russia.

¹¹Department of Physics, Clarendon Laboratory, Oxford, UK.

¹²NASA Langley Research Center, Hampton, Virginia, USA.

¹³Canadian Centre for Climate Modeling and Analysis, University of Victoria, Victoria, British Columbia, Canada.

¹⁴Météo-France, CNRM, Toulouse, France.

¹⁵NASA Goddard Institute for Space Studies, New York, New York, USA.

¹⁶Frontier Research Center for Global Change, Japan Agency for Marine-Earth Science and Technology, Yokohama, Japan.

¹⁷Meteorological Research Institute, Tsukuba, Japan.

¹⁸Physics Department, Imperial College, London, UK.

and Trenberth, 1997]. Radiative forcing can affect either the shortwave or longwave components of the radiative budget. The changes can be caused by a number of factors including variations in solar insolation, alteration in surface boundary conditions related to land use change and desertification, or natural and anthropogenic perturbations to the radiatively active species in the atmosphere. The most basic and most important forcings are related to anthropogenic increases in the well-mixed greenhouse gases (WMGHGs) CO_2 , CH_4 , N_2O , and the halocarbons. The WMGHGs enhance the absorption of radiation in the atmosphere through excitation of molecular rotational and rotational-vibrational modes by infrared and near-infrared photons. Despite continuing uncertainty regarding the magnitude of aerosol radiative forcing [Anderson et al., 2003], it is very likely that the net anthropogenic radiative forcing of the climate system is positive because of the effects of WMGHGs [Boucher and Haywood, 2001]. The increased concentrations of CO_2 , CH_4 , and N_2O between 1750 and 1998 have produced forcings of +1.48, +0.48, and +0.15 W m^{-2} , respectively [IPCC, 2001]. The introduction of halocarbons in the mid-20th century has contributed an additional +0.34 W m^{-2} , for a total forcing by WMGHGs of +2.45 W m^{-2} with a 15% margin of uncertainty. The positive sign of these forcings reflects the fact that the climate system is releasing less and absorbing more radiative energy than in its unperturbed state.

[3] Coupled atmosphere-ocean general circulation models (AOGCMs) [Trenberth, 1992; Randall, 2000] represent the most comprehensive systems for simulating the response of the climate to radiative forcings. AOGCMs have been used extensively to simulate change in response to WMGHGs and other agents since pioneering studies by Manabe and Wetherald [1975] and other modeling groups. In the current fourth Assessment Report (AR4) of the Intergovernmental Panel on Climate Change (IPCC), sixteen international groups are submitting simulations from 23 different AOGCMs. These simulations are used to project climate change in the recent past and in the future under a variety of emissions scenarios for WMGHGs and other radiative species [Nakicenovic and Swart, 2000].

[4] Because of the intrinsic complexity of the numerous processes included in these models and the computational demands of climate change simulation, it is frequently necessary to approximate the various processes using simplified representations called parameterizations. Such approximations are necessary both for processes grounded in first principles theory (e.g., radiative transfer) and for elements of the climate system which are less well understood (e.g., clouds). Radiative transfer is one physical process that can be calibrated against fiduciary methods in the form of highly accurate numerical solutions. These solutions can be employed to verify parameterizations of radiative effects in climate models. The lack of stringent observational or theoretical constraints on the second class of processes has resulted in a diversity of parameterizations for many components of the climate system. The use of a multimodel ensemble in the IPCC assessment reports is an attempt to characterize the impact of parameterization uncertainty on climate change predictions.

[5] The interaction of shortwave and longwave radiation with an (idealized) atmosphere free of clouds and aerosols

can be calculated to a very high degree of accuracy [Halothore et al., 2005]. The remaining uncertainties are related primarily to some aspects of the spectroscopy of the WMGHGs and other atmospheric constituents and to the treatment of broadband continuum absorption by H_2O , CO_2 , and other species. Very accurate line-by-line (LBL) codes can solve the basic equations of radiative transfer [Liou, 1992] for each quantum transition, or “line”, registered for each radiatively active molecular constituent in the atmosphere. In carefully controlled comparisons against field data, LBL results agree with measured spectra to within observational uncertainty [e.g., Tjemkes et al. 2003], although this agreement is, to some extent, due to empirical tuning of the water vapor continuum. Kratz et al. [2005] have shown that a collection of LBL models produce far-infrared radiances and fluxes that differ by roughly 0.5% when applied to identical atmospheric profiles. The results from LBL codes represent a rigorous set of benchmark calculations for development and evaluation of radiation codes in AOGCMs [Clough and Iacono, 1995].

[6] There have been several efforts to evaluate the accuracy of radiative parameterizations in AOGCMs relative to LBL calculations. The major projects include the Intercomparison of Radiation Codes in Climate Models (ICRCCM) [Ellingson and Fouquart, 1991; Ellingson et al., 1991; Fouquart et al., 1991], an intercomparison of forcing by ozone computed with various codes [Shine et al., 1995], the GCM Reality Intercomparison Project for SPARC (GRIPS) [Pawson et al., 2000], an assessment of treatments for unresolved clouds [Barker et al., 2003], and an intercomparison of shortwave codes and measurements [Halothore et al., 2005]. Heating rates have been previously evaluated by Fels et al. [1991]. Analysis of radiative forcing by WMGHGs derived from earlier generations of AOGCMs has uncovered large discrepancies relative to LBL calculations, for example in the forcing from doubling atmospheric concentrations of CO_2 [Cess et al., 1993]. The problems encountered in the Cess et al. [1993] study include omission of minor CO_2 absorption bands, errors in the overlap of absorption by H_2O and CO_2 , and unresolved issues with the formulation of longwave radiative transfer. Analyses of the radiative forcing by sulfate aerosols has also demonstrated large differences among models [Boucher et al., 1998].

[7] In this study, we update the earlier intercomparisons by evaluating many of the AOGCMs included in the IPCC AR4 (2007) (in preparation) against a representative set of current LBL codes. The goals of this exercise are to evaluate the fidelity of AOGCMs included in the IPCC AR4 and to establish new benchmark calculations for this purpose. The chief objective is to determine the differences in WMGHG forcing caused by the use of different radiation codes in the AOGCMs used for IPCC simulations of climate change. Unlike some of the previous studies, the emphasis here is on the accuracy of radiative forcing rather than radiative flux. While the effects of increasing WMGHGs represent only part of the forcing applied to the climate system, a comprehensive evaluation of all the forcing agents in AOGCMs is beyond the scope of this work.

[8] The Radiative Transfer Model Intercomparison Project (RTMIP) and the participating models are described in section 2. Results for the radiative forcings at the top of

Table 1. Atmospheric Constituents for the Radiative Calculations

Calculation	CO ₂ , ppmv	CH ₄ , ppbv	N ₂ O, ppbv	CFC-11, pptv	CFC-12, pptv	H ₂ O ^a
1a	287	0	0	0	0	1
2a	369	0	0	0	0	1
2b	574	0	0	0	0	1
3a	287	806	275	0	0	1
3b	369	1760	316	267	535	1
3c	369	1760	275	0	0	1
3d	369	806	316	0	0	1
4a	574	0	0	0	0	1.2

^aMultiplier applied to the H₂O mixing ratios in the AFGL MLS profile.

model (TOM), 200 hPa (a surrogate for the tropopause), and surface are presented in section 3.1. A comparison of the corresponding changes in atmospheric heating rates is given in section 3.2. Discussion and conclusions are presented in section 4.

2. Experimental Configuration

2.1. Clear-Sky Forcing Calculations

[9] The specific goal of this study is to quantify the differences in instantaneous radiative forcing calculated from AOGCM and LBL radiation codes. On the basis of experience from previous intercomparisons, the calculations requested from the participants in RTMIP are not sufficient for detailed explanation of the differences. On the other hand, minimizing the number of required calculations has helped insure nearly unanimous participation by the AOGCM groups.

[10] The calculations are performed off line by applying the LBL codes and radiative parameterizations from the AOGCMs to a specified atmospheric profile. The results are therefore not affected by differences among the atmospheric climatologies produced by the various AOGCMs. The radiatively active species included in this evaluation are the WMGHGs CO₂, CH₄, N₂O, and the chlorofluorocarbons CFC-11 and CFC-12. The intercomparison is based upon calculations of the instantaneous changes in clear-sky fluxes when concentrations of these WMGHGs are perturbed. While the relevant quantity for climate change is all-sky forcing, the introduction of clouds would greatly complicate the intercomparison exercise and therefore clouds are omitted from RTMIP.

[11] In addition, the calculations omit the effects of stratospheric thermal adjustment to forcing derived using fixed dynamical heating (FDH) [Ramanathan and Dickinson, 1979; Fels et al., 1980]. This omission facilitates

comparison of fluxes from LBL codes and AOGCM parameterizations. For the purposes of this intercomparison, “flux” is defined as “flux for clear-sky and aerosol-free conditions” and “forcing” is defined as “instantaneous changes in fluxes without stratospheric adjustment”. It should be noted that our omission of FDH means that the results in this study are not directly comparable to the estimates of forcing at the tropopause in the IPCC [2001] reports, since the latter include the effects of adjustment. The effects of adjustment on forcing are approximately −2% for CH₄, −4% for N₂O, +5% for CFC-11, +8% for CFC-12, and −13% for CO₂ [IPCC, 1995; Hansen et al., 1997].

[12] The specifications for each of the calculations requested from the LBL and AOGCM groups are given in Table 1. The concentrations of WMGHGs in calculations 3a and 3b correspond to conditions in the years 1860 AD and 2000 AD, respectively. The concentrations in 1860 are obtained from a variety of sources detailed in IPCC [2001]. Differences among these calculations cover several standard forcing scenarios performed by all AOGCMs in the AR4, including (1) forcing for changes in CO₂ concentrations from 1860 to 2000 values (case 2a-1a) and from 1860 to double 1860 values (case 2b-1a), (2) forcing for changes in WMGHGs from 1860 to 2000 values (case 3b-3a), and (3) the effect of increased H₂O predicted when CO₂ is doubled (case 4a-2b). In addition to the four forcing experiments listed above, there are three additional forcing experiments for combinations of CH₄, N₂O, CFC-11, and CFC-12. The changes in WMGHGs and H₂O in these seven forcing experiments are listed in Table 2.

[13] The quantities requested from each participating group include (1) net shortwave and longwave clear-sky flux at the top of the model, (2) net shortwave and longwave clear-sky flux at 200 hPa, (3) net shortwave and longwave clear-sky flux at the surface, and (4) (optionally) net shortwave and longwave clear-sky fluxes at each layer interface in the profile. The reason for performing calculations at 200 hPa rather than the tropopause is to insure consistency with the radiative quantities requested as part of the climate change simulations. Since not all modeling groups are prepared to compute fluxes at a time-evolving tropopause, the Working Group on Coupled Modeling (WGCM) of the World Climate Research Programme (WCRP) and the IPCC have requested fluxes at a surrogate for the tropopause at the 200 hPa pressure surface. The precise choice of tropopause can affect forcings by up to 10% [Myhre and Stordal, 1997].

[14] In order to establish a common baseline, the background atmospheric state for all the calculations is a

Table 2. Changes in Atmospheric Constituents for Forcing Calculations

Case ^a	CO ₂ , ppmv	CH ₄ , ppbv	N ₂ O, ppbv	CFC-11, pptv	CFC-12, pptv	H ₂ O ^b
2a-1a	287 → 369	–	–	–	–	–
2b-1a	287 → 574	–	–	–	–	–
3b-3a	287 → 369	806 → 1760	275 → 316	0 → 267	0 → 535	–
3a-1a	–	0 → 806	0 → 275	–	–	–
3b-3c	–	–	275 → 316	0 → 267	0 → 535	–
3b-3d	–	806 → 1760	–	0 → 267	0 → 535	–
4a-2b	–	–	–	–	–	1 → 1.2

^aDifferences between calculations in Table 1.

^bChange in multiplier applied to the H₂O mixing ratios in the AFGL MLS profile.

Table 3. Sensitivity of TOM and Surface Forcings to Features of the Calculations^a

Band	Feature	$\langle \delta F_{TOM}(\text{Band}) \rangle$, W m ⁻²	$\langle \delta F_{SRF}(\text{Band}) \rangle$, W m ⁻²
LW	vertical resolution	-0.011 ± 0.017	-0.004 ± 0.009
LW	temperature interpolation	0.011 ± 0.020	0.016 ± 0.013
SW	O ₂ absorption	0.000 ± 0.001	0.001 ± 0.003

^aParameters $\langle \delta F_{TOM}(\text{Band}) \rangle$ and $\langle \delta F_{SRF}(\text{Band}) \rangle$ are the mean changes in TOM and surface forcing when features of the forcing calculation are changed. The mean changes are averages across the seven forcing cases listed in Table 2. The longwave (LW) sensitivities are calculated using the NASA MRTA model (Table 6), and the shortwave (SW) sensitivities are calculated using the NCAR CCSM3 radiative parameterization (Table 4).

climatological midlatitude summer (MLS) atmospheric profile [Anderson *et al.*, 1986]. Therefore all the calculations are performed using the same vertical profiles of temperature and the mixing ratio of O₃. The profile of specific humidity is also held fixed except for calculation 4a (Table 1). The concentrations of WMGHGs are set to a constant mixing ratio with respect to dry air throughout the column. The standard MLS profile has been interpolated to 40 levels for the AOGCM groups and 459 levels for the LBL groups. As shown in Table 3, the comparison of forcings from AOGCM and LBL codes is not affected by the difference in resolution. Increasing resolution from 40 to 459 levels changes the longwave forcings at TOM and surface by less than approximately 0.01 W m⁻². Changing the methods of temperature interpolation within each layer in the LBL calculations changes the longwave forcings by less than 0.02 W m⁻². The input profiles are available from the RTMIP Web site at <http://www.cgd.ucar.edu/RTMIP/>.

[15] The main radiative effects of atmospheric species included in the calculations are molecular Rayleigh scattering and the absorption by the WMGHGs, H₂O, and O₃. There is also a reduction in O₂ stoichiometrically equivalent to the increase in CO₂. The forcing calculations should not be appreciably affected by the red and near-infrared (A, B, and γ) bands of O₂, collisionally induced rotation bands in N₂ at approximately 100 μ m, quadrupole transitions in the fundamental vibration band of N₂ at 4.3 μ m, the forbidden transitions of O₂ in the vibration-rotation band, or the collision complexes O₂ · O₂ and O₂ · N₂. For example, the effect of the A, B, and γ bands of O₂ on the shortwave forcing is less than 0.001 W m⁻² (Table 3). The inclusion or

omission of these absorption bands has been left to the discretion of the individual AOGCM and LBL modelers. The LBL groups have used spectral ranges of 4 to 100 μ m for the longwave and 0.2 to 5 μ m for the shortwave. The spectral interval of 4 to 5 μ m is contained in both shortwave and longwave calculations, but it is not counted twice since the shortwave codes omit thermal emission and the longwave codes omit solar flux. Some of the LBL groups have provided their spectrally resolved fluxes corresponding to their broadband calculations. The AOGCM groups have been asked to use the standard spectral ranges for their respective radiative parameterizations.

[16] For the shortwave calculations, the surface is a Lambertian reflector with a spectrally flat albedo of 0.1. At the TOM, the solar radiation is set to 1360 W m⁻² incident at a zenith angle of 53 degrees. The value for TOM solar insolation is the difference between a broadband solar constant of 1367 W m⁻² and the 6.33 W m⁻² of insolation in wavelengths larger than 5 μ m excluded from the calculations [Labs and Neckel, 1970]. This radiation is excluded since most AOGCM shortwave parameterizations do not treat this wavelength range. For the longwave calculations, the surface is assumed to have a spectrally flat emissivity equal to 1 and a thermodynamic temperature of 294 K.

2.2. General Circulation and Line-by-Line Models

[17] The AOGCM groups and models contributing calculations to RTMIP are listed in Tables 4 and 5. There are 16 groups submitting simulations to the IPCC AR4, and fourteen of these are participating in RTMIP. The groups have submitted simulations from 23 models to the IPCC

Table 4. AOGCMs in the Intercomparison

Originating Group ^a	Country	Model
BCCR	Norway	BCCR-BCM2.0
CCCma	Canada	CGCM3.1(T47/T63)
CCSR/NIES/FRCGC	Japan	MIROC3.2(medres/hires)
CNRM	France	CNRM-CM3
GFDL	USA	GFDL-CM2.0/2.1
GISS	USA	GISS-EH/ER
INM	Russia	INM-CM3.0
IPSL	France	IPSL-CM4
LASG/IAP	China	FGOALS-g1.0
MIUB/METRI/KMA	Germany/Korea	ECHO-G
MPIfM	Germany	ECHAM5/MPI-OM
MRI	Japan	MRI-CGCM2.3.2
NCAR	USA	CCSM3
NCAR	USA	PCM
UKMO	UK	HadCM3
UKMO	UK	HadGEM1

^aThe acronyms for the groups are given in Table 5.

Table 5. Acronyms for Modeling Groups

Acronym	Originating Group
BCCR	Bjerknes Centre for Climate Research
CCCma	Canadian Centre for Climate Modeling and Analysis
CCSR	Center for Climate System Research (The University of Tokyo)
CNRM	Centre National de Recherches Météorologiques (Météo-France)
FRCGC	Frontier Research Center for Global Change (JAMSTEC)
GFDL	Geophysical Fluid Dynamics Laboratory (NOAA)
GISS	Goddard Institute for Space Studies (NASA)
IAP	Institute of Atmospheric Physics
ICSTM	Imperial College of Science, Technology, and Medicine
INM	Institute for Numerical Mathematics
IPSL	Institut Pierre Simon Laplace
JAMSTEC	Japan Agency for Marine-Earth Science and Technology
LARC	Langley Research Center (NASA)
LASG	Laboratory of Numerical Modeling for Atmospheric Sciences and Geophysical Fluid Dynamics
MPiFm	Max Planck Institute for Meteorology
MRI	Meteorological Research Institute
MIUB	Meteorological Institute of the University of Bonn
METRI/KMA	Meteorological Research Institute, Korean Meteorological Administration
NCAR	National Center for Atmospheric Research
NIES	National Institute for Environmental Studies
UKMO	Met Office's Hadley Centre for Climate Prediction and Research
UR	University of Reading

data archive, and calculations representing twenty of these are included in our intercomparison. It should be noted that a number of the AOGCMS have similar or identical radiative parameterizations. The two AOGCMS developed by each of the groups CCCma, CCSR/NIES/FRCGC, GFDL, and GISS share common radiation codes. Each pair of models is represented by a single set of calculations in RTMIP. In addition, the models BCCR-BCM2.0 and CNRM-CM3 have identical parameterizations, and the treatments of trace gases in CCSM3, FGOALS-g1.0 and PCM are essentially the same. The characteristics of the radiative parameterizations used in many of these AOGCMS are described in detail by Q. Fu and V. Ramaswamy (manuscript in preparation, 2006).

[18] The LBL groups contributing calculations to RTMIP are listed in Tables 5 and 6. The details of the calculations performed with each LBL code are given in Table 7. The five participating LBL groups have each performed the longwave calculations, and four excepting LARC have performed the shortwave calculations. The LBL models are all based upon the same Hitran line database for radiatively active species [Rothman *et al.*, 2003], although three of the models include additional corrections to that database. Because of the heterogeneity of LBL configurations shown in Table 7, the agreement among the absolute fluxes from these codes is not as good as the agreement that can be achieved in more rigorously controlled intercomparisons [e.g., Kratz *et al.*, 2005]. However, the objective in RTMIP is to derive accurate forcings, and the set of LBL

calculations is adequate for that application (section 3). The reason is that any offsets in the fluxes from a particular LBL code are sufficiently constant across the various calculations that the offsets cancel when differencing these calculations to derive the forcings. For example, consider the 200 hPa longwave fluxes $F_{200}(LW)$ for calculations 1a and 2a. The difference between these fluxes is the longwave forcing at 200 hPa caused by an increase in CO_2 from 287 to 369 ppmv (Table 2). For both of the calculations 1a and 2a, the standard deviation of the five LBL estimates of $F_{200}(LW)$ is 1.25 W m^{-2} . However, the standard deviation of the forcing (the difference between calculations 1a and 2a) is just 0.02 W m^{-2} . This example illustrates that discrepancies among LBL radiative codes that affect the calculation of fluxes need not appreciably affect the calculation of forcings. The results from the LBL codes are available from the RTMIP Web site at <http://www.cgd.ucar.edu/RTMIP/>.

[19] Sample longwave forcing calculations with the Reference Forward Model (RFM) (Tables 6 and 7) are shown in Figure 1. The ratio of the net longwave flux at 200 hPa to the longwave upward flux from the surface is plotted in Figure 1 (top). Values close to 1 indicate that radiation reaching 200 hPa originates from the surface or near the surface, while values close to 0 result from a combination of strong absorption and the thermal stratification of the troposphere [Goody and Yung, 1989]. The four prominent features are the strong H_2O band at $6.3 \mu\text{m}$, the midinfrared “window” between 8 and $12 \mu\text{m}$, the CO_2 band at $15 \mu\text{m}$,

Table 6. LBL Radiation Codes in the Intercomparison

Originating Group ^a	Country	Model	Reference
GFDL	USA	GFDL LBL	Schwarzkopf and Fels [1985]
GISS	USA	LBL3	–
ICSTM	UK	GENLN2	Edwards [1992]; Zhong <i>et al.</i> [2001]
LARC	USA	MRTA	Kratz and Rose [1999]
UR	UK	RFM	Dudhia [1997] and Stannnes <i>et al.</i> [1988]

^aThe acronyms for the groups are given in Table 5.

Table 7. Characteristics of the LBL Radiation Calculations^a

Group	Line Data	Line Updates	H ₂ O Cont.	CO ₂ Cont.	SW Res., cm ⁻¹	SW Solver	SW Stream	LW Res., cm ⁻¹	LW Solver
GFDL	H2K	H2001	CKD2.4	None	–	A/D	32	0.0001/0.1	G
GISS	H2K	None	Tipping/Ma	None	0.01/0.1	A/D	1	0.000125/0.0025	G
ICSTM	H2K	Voigt	CKD2.2	GENLN	0.01	–	2	0.002	5-pt. G
LARC	H2K	None	MT-CKD1.0	MT-CKD1.0	–	–	–	0.005	8-pt. G
UR	H2K	H2001	CKD2.4.1	RFM	0.005	DISORT	4	0.0025	G

^aAbbreviations and references are as follows: H2K and H2001 are the Hitran 2000 database and its updates in 2001 [Rothman *et al.*, 2003]; updates are corrections or additions to a particular line database; Voigt is a compilation of ozone absorption cross-sections [Voigt *et al.*, 2001]; “Cont.” is an abbreviation for continuum; CKD is the Clough-Kneizys-Davies continuum [Clough *et al.*, 1989]; Tipping/Ma refers to their continuum [Tipping and Ma, 1995]; MT-CKD is the Mlawer-Tobin update to CKD [Clough *et al.*, 2005]; GENLN is the General Line-by-Line Atmospheric Transmittance and Radiance Model [Edwards, 1992]; RFM is the Reference Forward Model based upon GENLN [Dudhia, 1997]; “Res.” is an abbreviation for (spectral) resolution; “Solver” is the technique or software used to solve the integro-differential radiative transfer equations (RTEs); “Stream” is the number of zenith angles used for the quadrature approximation to the scattering operator in the RTEs; A/D is the adding-doubling method [Liou, 1992]; DISORT is the discrete ordinate radiative transfer package [Stammes *et al.*, 1988]; G is Gaussian quadrature; and “pt.” is an abbreviation for the number of points in the Gaussian quadrature [Liou, 1992].

and the far-infrared rotation band of H₂O [Liou, 1992]. The longwave forcings for four of the experiments in Table 2 are plotted in Figure 1 (bottom). As Figure 1 illustrates, the largest forcings generally occur outside the band centers of the major absorbing species. For example, the largest CO₂ forcings appear in the wings of the 15 μm band [e.g., IPCC 1995, Figure 4.1]. Similarly, the largest H₂O forcings occur in the midinfrared window and the far infrared, not in the 6.3 μm H₂O band. The reason is that the absorption in the band centers is effectively saturated, and therefore increases in radiatively active species have minimal effects at those wavelengths.

[20] Corresponding shortwave forcing calculations performed with the RFM are shown in Figure 2. The ratio of the net surface flux to the TOM solar radiation is plotted in Figure 2 (top). At wavelengths where the ratio is close to 1, the atmosphere transmits most of the incident flux to the surface [Goody and Yung, 1989]. Where the ratio is close to 0, the incident flux is largely absorbed by trace gases and water vapor along the ray path from the top of atmosphere to the surface. The major features in the transmission spectrum are the extremely strong O₃ bands at wavelengths below 0.26 μm, the visible atmospheric “window” between 0.3 and 0.7 μm, the CO₂ bands at 2.7 and 4.3 μm, and the primary and overtone bands of H₂O [Liou, 1992]. The shortwave forcings for four of the experiments in Table 2 are plotted in Figure 2 (right). Because of saturation effects, there is virtually no forcing near the CO₂ and H₂O band centers at 2.7 μm or the middle of the CO₂ band at 4.3 μm. However, in other near-infrared bands of H₂O and the WMGHGs, the line strengths are sufficiently weak that forcing can occur near the band centers. An example is the forcing by H₂O in its overtone bands at wavelengths below 2 μm [Ramaswamy and Freidenreich, 1998]. It is also evident from comparison of the ordinates in Figures 1 (right) and 2 (right) that the forcings by WMGHGs in the near infrared are generally weaker than the forcings in the middle and far infrared.

3. Comparison of Calculations from AOGCMs and LBL Models

3.1. Forcings From AOGCMs and LBL Models

[21] The statistical summaries of the forcing intercomparison are given in Table 8 for the longwave and Table 9 for the shortwave. For each level, Tables 8 and 9 list the mean

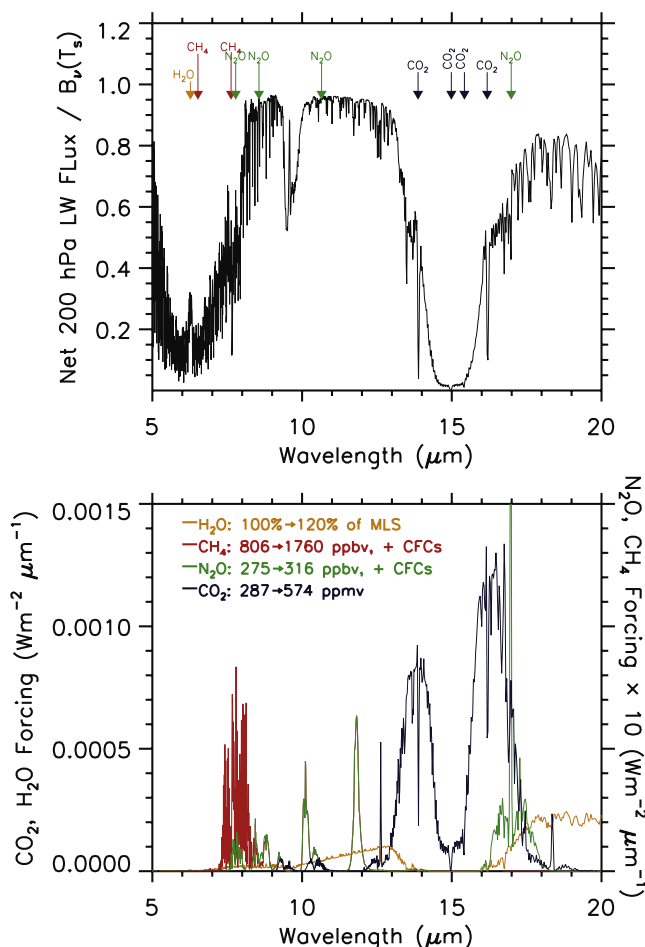


Figure 1. (top) Net upward longwave flux at 200 hPa for year 2000 WMGHGs (calculation 3b, Table 1) divided by the surface Planck function versus wavelength. Blue, green, red, and yellow arrows indicate the principal infrared absorption bands of CO₂, N₂O, CH₄, and H₂O, respectively. (bottom) Longwave radiative forcing at 200 hPa by CO₂ (case 2b-1a, Table 2), N₂O and CFCs (case 3b-3c), CH₄ and CFCs (case 3b-3d), and H₂O (case 4a-2b).

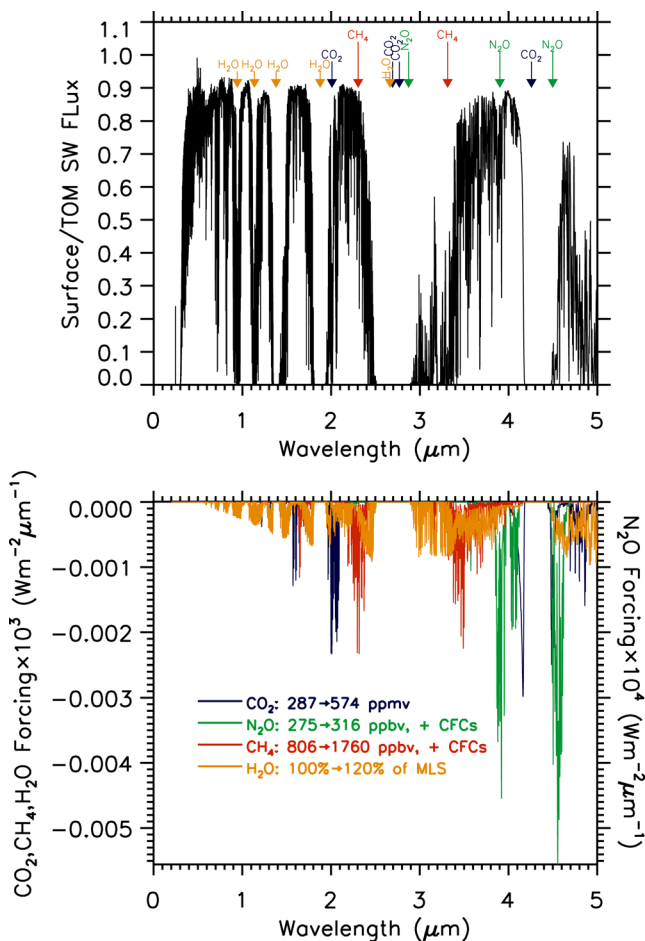


Figure 2. (top) Net downward surface shortwave flux for year 2000 WMGHGs (calculation 3b, Table 1) divided by TOM incident solar flux versus wavelength. Blue, green, red, and yellow arrows indicate the principal near-infrared absorption bands of CO_2 , N_2O , CH_4 , and H_2O , respectively. (bottom) Shortwave radiative forcing at the surface by CO_2 (case 2b-1a, Table 2), N_2O (case 3b-3c), CH_4 (case 3b-3d), and H_2O (case 4a-2b).

and standard deviation of the AOGCM and LBL results and the difference between the means. Tables 8 and 9 also show the probability from the Student's *t* test that the ensembles of AOGCM and LBL forcings have different means if the (hypothetical) parent distributions of AOGCM and LBL forcings have the same means. In the following discussion, the differences between the AOGCM and LBL results will be characterized as significant if the *t* test probability is less than 0.01. There are sixteen members in the ensemble of forcings from AOGCMs (Table 4), although not all of the radiative transfer parameterizations in these models are independent (section 2.2). Therefore the Student's *t* test results are biased somewhat high by an overestimate of the number of truly independent AOGCM calculations. For the LBL models, there are five members of the longwave forcing ensemble and four members of the shortwave forcing ensemble.

[22] The results from each of the forcing experiments are shown in Figures 3–9. The left and right panels in

Figures 3–9 display the longwave and shortwave forcing statistics, respectively. The data from AOGCMs are shown with box-and-whisker diagrams [Tukey, 1977] for the three mandatory levels in the intercomparison. Since there are fewer LBL models, only the minimum, median, and maximum LBL values are plotted for each level. In many cases, the range of LBL estimates is so small compared to the scale of the abscissa that it is not visible in the plot, for example in the graph of shortwave forcing from doubling CO_2 (Figure 3, right).

[23] Perhaps the most basic result of the intercomparison is that all the mean forcings from averages over the ensemble of AOGCMs have the same sign as the corresponding mean LBL forcings. With one single exception, the individual forcing values from each AOGCM also have the same signs as the equivalent LBL forcings. The exception occurs for one of the AOGCMs in the increased H_2O experiment (case 4a-2b) in the shortwave band at the 200 hPa level. The longwave forcings are uniformly positive for all mandatory levels and for all experiments. The effect of increased WMGHGs and H_2O is to reduce the net upward longwave flux from the atmosphere and surface below. The LBL shortwave forcings are positive or zero at the TOM and uniformly negative at the surface. This implies that WMGHGs and H_2O enhance the absorption of solar radiation by the surface-atmosphere column. However, since the additional absorption occurs in the atmosphere and primarily affects the downwelling direct beam radiation, the higher absorption also reduces the net surface insolation. This does not necessarily imply a cooling effect on the surface climate because of coupling between the surface and troposphere.

[24] The forcing by increased CO_2 is the most important component of the total forcing of the climate in the recent past. The model estimates for the shortwave and longwave effects from the observed increase and from doubling CO_2 are shown in Figures 3 and 4. The AOGCMs tend to underestimate the longwave forcing at the three mandatory levels. The biases relative to LBL codes, while not large in relative terms, are statistically significant (Table 8). The relative differences in the mean forcings are less than 8% for the pseudotropopause at 200 hPa, but increase to approximately 13% at the TOM and to 33% at the surface. The small errors at 200 hPa may reflect earlier efforts to improve the accuracy of AOGCM calculations of radiative forcing at the tropopause. In general, the mean shortwave forcings from the LBL and AOGCM codes are in good agreement at all three mandatory levels. This implies the differences between the mean shortwave forcings for increased WMGHGs from 1860 to 2000 are not related to errors in the treatment of CO_2 . However, the range in shortwave forcing at the surface from individual AOGCMs is quite large. The ratios of the standard deviations to the mean forcings, or coefficients of variation, for the two cases are 0.94 and 0.95 (Table 9). In addition, one of the AOGCM shortwave parameterizations does not include the effects of CO_2 on shortwave fluxes and heating rates. The omission explains why the box-and-whisker diagrams for the multi-AOGCM ensemble of shortwave calculations in Figures 3 and 4 intersect the zero forcing value on the abscissas. This particular model only computes a nonzero shortwave forcing in case 4a-2b for increased H_2O .

Table 8. Longwave Forcing^a

Level	Field	Forcing Cases						
		2a-1a	2b-1a	3b-3a	3a-1a	3b-3c	3b-3d	4a-2b
Figure		3	4	5	6	7	8	9
TOM	$\langle F_{gcm} \rangle$	0.88	2.45	2.19	3.61	0.59	1.10	3.57
TOM	$\sigma(F_{gcm})$	0.13	0.35	0.30	0.82	0.23	0.26	0.46
TOM	$\langle F_{lbl} \rangle$	1.01	2.80	2.09	3.63	0.48	0.93	3.78
TOM	$\sigma(F_{lbl})$	0.02	0.06	0.13	0.05	0.14	0.14	0.09
TOM	$\langle F_{gcm} \rangle - \langle F_{lbl} \rangle$	-0.13	-0.35	0.10	-0.02	0.10	0.17	-0.20
TOM	$p(F_{gcm}, F_{lbl})$	0.001	0.001	0.305	0.938	0.254	0.077	0.116
200 hPa	$\langle F_{gcm} \rangle$	1.82	5.07	2.95	3.37	0.47	0.95	4.45
200 hPa	$\sigma(F_{gcm})$	0.17	0.43	0.32	0.73	0.15	0.30	0.39
200 hPa	$\langle F_{lbl} \rangle$	1.95	5.48	3.00	3.47	0.41	0.89	4.57
200 hPa	$\sigma(F_{lbl})$	0.02	0.07	0.10	0.03	0.11	0.12	0.14
200 hPa	$\langle F_{gcm} \rangle - \langle F_{lbl} \rangle$	-0.13	-0.42	-0.06	-0.10	0.06	0.06	-0.11
200 hPa	$p(F_{gcm}, F_{lbl})$	0.008	0.002	0.544	0.595	0.393	0.486	0.334
Surface	$\langle F_{gcm} \rangle$	0.38	1.12	1.21	1.80	0.43	0.74	11.95
Surface	$\sigma(F_{gcm})$	0.13	0.39	0.38	0.87	0.18	0.28	0.75
Surface	$\langle F_{lbl} \rangle$	0.57	1.64	1.08	1.14	0.28	0.46	11.52
Surface	$\sigma(F_{lbl})$	0.02	0.04	0.12	0.05	0.11	0.11	0.40
Surface	$\langle F_{gcm} \rangle - \langle F_{lbl} \rangle$	-0.19	-0.52	0.12	0.67	0.15	0.28	0.43
Surface	$p(F_{gcm}, F_{lbl})$	0.000	0.000	0.285	0.008	0.044	0.005	0.121

^a $\langle F \rangle$ and $\sigma(F)$ are the mean and standard deviation of an ensemble of forcings F ; $p(F_1, F_2)$ is the Student's t test probability that the ensembles F_1 and F_2 have different means if the parent distributions of F_1 and F_2 have the same mean; F_{gcm} and F_{lbl} are the ensembles of forcings from the AOGCMs and LBL models. Forcing cases are from Table 2. Values are in $W m^{-2}$.

[25] The forcing applied to the climate from increases in WMGHGs between 1860 and 2000 is shown in Figure 5. In the longwave, the differences between the mean forcings calculated with AOGCMs and LBL models are not statistically significant at the three surfaces included in the intercomparison (Table 8). This agreement results in part from compensating errors in the AOGCM codes. Nonetheless, this is perhaps the most important test for the accuracy of the forcing applied to the AOGCMs in simulations of the

recent past, leading to the simulated warming in the 20th century. In the shortwave, the AOGCMs systematically underestimate the magnitude of the forcings at the three mandatory levels, and the differences are highly significant (Table 9). As the following analysis will show, the discrepancies are caused by the omission of CH_4 and N_2O from all of the AOGCM radiative parameterizations.

[26] The combined effects of increasing CH_4 and N_2O from 0 ppbv to the concentrations of these gases at 1860 are

Table 9. Shortwave Forcing^a

Level	Field	Forcing Cases						
		2a-1a	2b-1a	3b-3a	3a-1a	3b-3c	3b-3d	4a-2b
Figure		3	4	5	6	7	8	9
TOM	$\langle F_{gcm} \rangle$	0.07	0.21	0.07	0.00	0.00	0.00	0.63
TOM	$\sigma(F_{gcm})$	0.07	0.21	0.07	0.00	0.00	0.00	0.21
TOM	$\langle F_{lbl} \rangle$	0.04	0.12	0.13	0.15	0.00	0.09	0.75
TOM	$\sigma(F_{lbl})$	0.00	0.01	0.00	0.01	0.00	0.00	0.01
TOM	$\langle F_{gcm} \rangle - \langle F_{lbl} \rangle$ TOM	0.03	0.08	-0.06	-0.15	-0.00	-0.09	-0.12
TOM	$p(F_{gcm}, F_{lbl})$	0.138	0.141	0.004	0.000	0.235	0.000	0.039
200 hPa	$\langle F_{gcm} \rangle$	-0.27	-0.79	-0.27	0.00	0.00	0.00	0.37
200 hPa	$\sigma(F_{gcm})$	0.09	0.28	0.09	0.00	0.00	0.00	0.23
200 hPa	$\langle F_{lbl} \rangle$	-0.27	-0.77	-0.41	-0.35	-0.02	-0.13	0.51
200 hPa	$\sigma(F_{lbl})$	0.01	0.02	0.01	0.01	0.01	0.00	0.01
200 hPa	$\langle F_{gcm} \rangle - \langle F_{lbl} \rangle$ 200 hPa	0.00	-0.02	0.14	0.35	0.02	0.13	-0.13
200 hPa	$p(F_{gcm}, F_{lbl})$	0.959	0.768	0.000	0.000	0.008	0.000	0.036
Surface	$\langle F_{gcm} \rangle$	-0.49	-1.47	-0.49	0.00	0.00	0.00	-4.89
Surface	$\sigma(F_{gcm})$	0.46	1.40	0.46	0.00	0.00	0.00	0.98
Surface	$\langle F_{lbl} \rangle$	-0.32	-0.96	-0.86	-0.95	-0.02	-0.53	-5.87
Surface	$\sigma(F_{lbl})$	0.01	0.02	0.02	0.04	0.00	0.02	0.31
Surface	$\langle F_{gcm} \rangle - \langle F_{lbl} \rangle$ Surface	-0.18	-0.50	0.37	0.95	0.02	0.53	0.98
Surface	$p(F_{gcm}, F_{lbl})$	0.144	0.170	0.006	0.000	0.002	0.000	0.004

^a $\langle F \rangle$ and $\sigma(F)$ are the mean and standard deviation of a sample of forcings F ; $p(F_1, F_2)$ is the Student's t test probability that the samples F_1 and F_2 have different means if the parent distributions of F_1 and F_2 have the same mean; F_{gcm} and F_{lbl} are the samples of forcings from the AOGCMs and LBL models. Forcing cases are from Table 2. Values are in $W m^{-2}$.

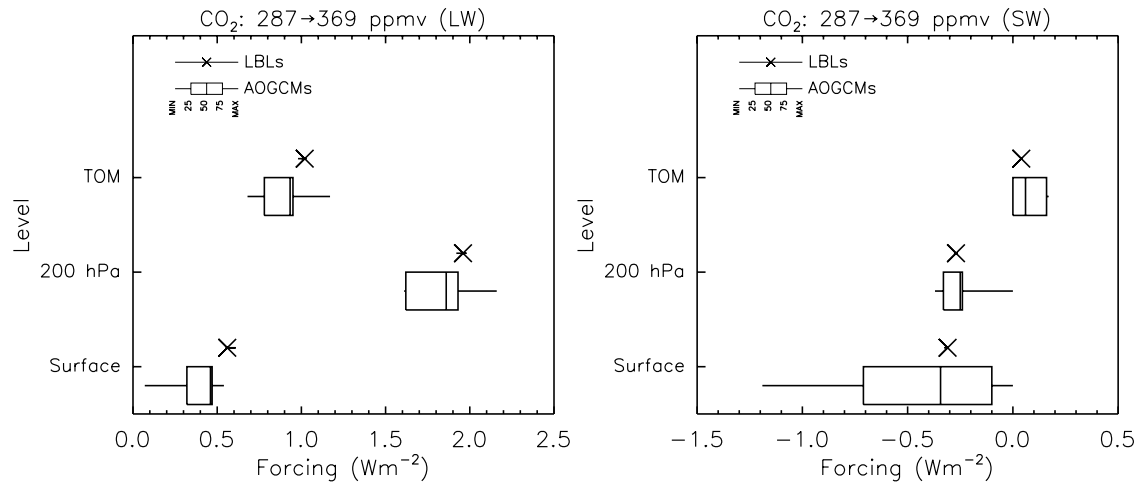


Figure 3. (left) Longwave forcings at TOM, 200 hPa, and the surface for increasing CO₂ from 287 to 369 ppmv (case 2a-1a, Table 2). AOGCM forcings are shown as box-and-whisker diagrams with percentiles given in the legend. The minimum-to-maximum range and median are plotted for the LBL codes. (right) Corresponding shortwave forcings.

plotted in Figure 6. The forcings from increasing N₂O and CFCs from concentrations at 1860 to 2000 are shown in Figure 7, and the corresponding forcings from increasing CH₄ and CFCs are shown in Figure 8. The absorption by CFC-11 and CFC-12 occurs almost entirely between 5 and 22.2 μm [e.g., Christidis *et al.*, 1997] and therefore shortwave forcing by these compounds may be neglected. As Figures 6–8 clearly show, all of the AOGCM codes in this intercomparison omit the effects of CH₄ and N₂O on shortwave fluxes and forcings. While the omission of N₂O does not introduce a large absolute error in the forcings, recent increases in CH₄ produce decreases of up to -0.5 W m^{-2} in the net shortwave fluxes at the surface in the LBL calculations (S. Freidenreich, personal communication, 2004). The AOGCMs also tend to overestimate the longwave forcing at the surface by both N₂O and CH₄, and these differences are statistically significant (Table 8). It is also evident from Figures 7 and 8 that the ranges of LBL longwave forcings for these cases are generally larger than

the corresponding ranges for the other cases. When CH₄ and N₂O are paired with CFC-11 and CFC-12, the spread in LBL longwave forcings at each of the mandatory levels is larger by at least 2 times than the corresponding range in the LBL calculation with CH₄ and N₂O alone (Table 8). In addition, the spread in the LBL results for N₂O combined with the CFCs is nearly identical to the spread for CH₄ combined with the CFCs. These results indicate that the divergence among LBL codes is related to the introduction of chlorofluorocarbons in the longwave calculations. While the discrepancy has been traced to one of the LBL codes in the intercomparison, the cause of the discrepancy has not been determined at this time. The authors and LBL developers are continuing to investigate this issue. These results imply that inaccuracies in the treatment of forcing by trace gases other than CO₂ need further systematic analysis.

[27] The longwave forcing from increasing H₂O is quite well simulated with the AOGCM codes (Figure 9). The

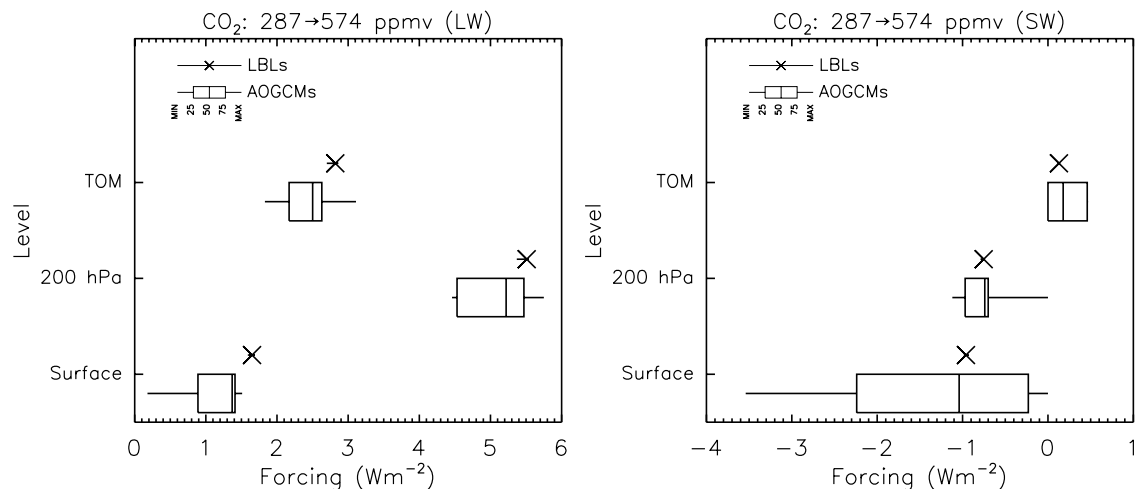


Figure 4. (left) Longwave forcings at TOM, 200 hPa, and the surface for increasing CO₂ from 287 to 574 ppmv (case 2b-1a, Table 2; same symbols as Figure 3). (right) Corresponding shortwave forcings.

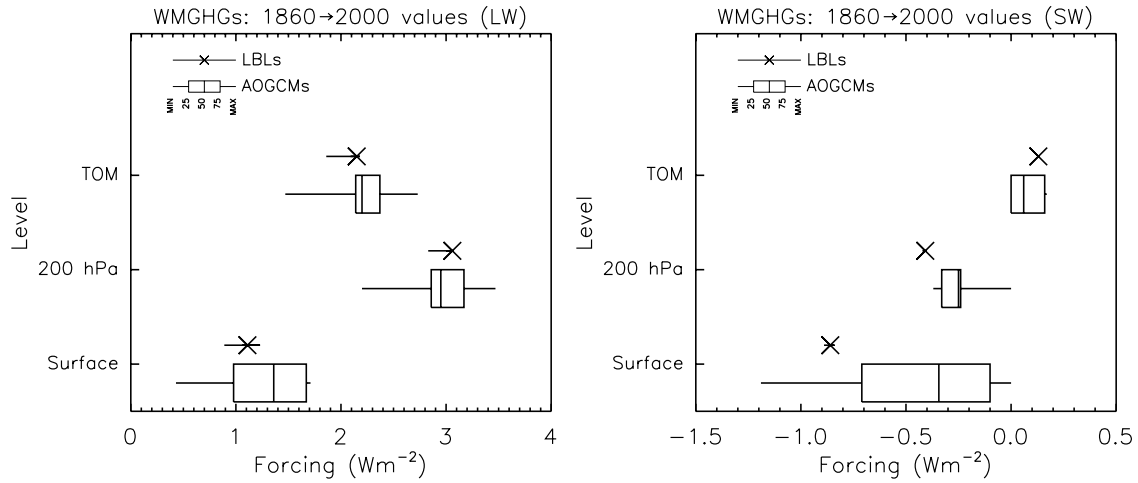


Figure 5. (left) Longwave forcings at TOM, 200 hPa, and the surface for increasing WMGHGs from year 1860 to year 2000 concentrations (case 3b-3a, Table 2; same symbols as Figure 3). (right) Corresponding shortwave forcings.

differences relative to the LBL calculations at the three standard levels are not statistically significant. In the shortwave, the only significant difference between the AOGCM and LBL calculations occurs at the surface, where the AOGCMs tend to underestimate the magnitude of the reduction in insolation. The single sign error in the individual AOGCM forcings relative to the LBL estimates occurs in the shortwave forcing at 200 hPa. The error is evident in the extension of the corresponding box-and-whisker diagram to negative values in Figure 9 (right). The fact that the surface forcing from the H₂O feedback is larger than the surface forcing by the WMGHGs is consistent with earlier modeling studies of the interactions of the hydrological cycle and anthropogenic climate change [e.g., Ramanathan, 1981].

3.2. Heating Rates From AOGCMs and LBL Models

[28] The perturbations to the heating rates by increases in WMGHGs and H₂O are relatively small. The first law of

thermodynamics applied to just the radiative processes in a vertically stratified atmosphere is:

$$\rho c_p \frac{\partial T}{\partial t} = -\frac{\partial F}{\partial z} \tag{1}$$

where ρ is the density of the atmosphere, c_p is the specific heat of air at constant pressure, T is the atmospheric temperature, F is a net radiative flux (positive upward), t is time, and z is the vertical coordinate. The radiative heating rates Q are equal to $\partial T/\partial t$ with time expressed in days. Integrating this equation over the depth of a standard atmosphere and denoting the mass-weighted heating rate by \bar{Q} gives

$$\bar{Q} \simeq \frac{\Delta F}{120} \tag{2}$$

with \bar{Q} expressed in units of K/day and the radiative flux convergence ΔF expressed in $W m^{-2}$. This same relationship applies when \bar{Q} and ΔF are perturbed by changes in

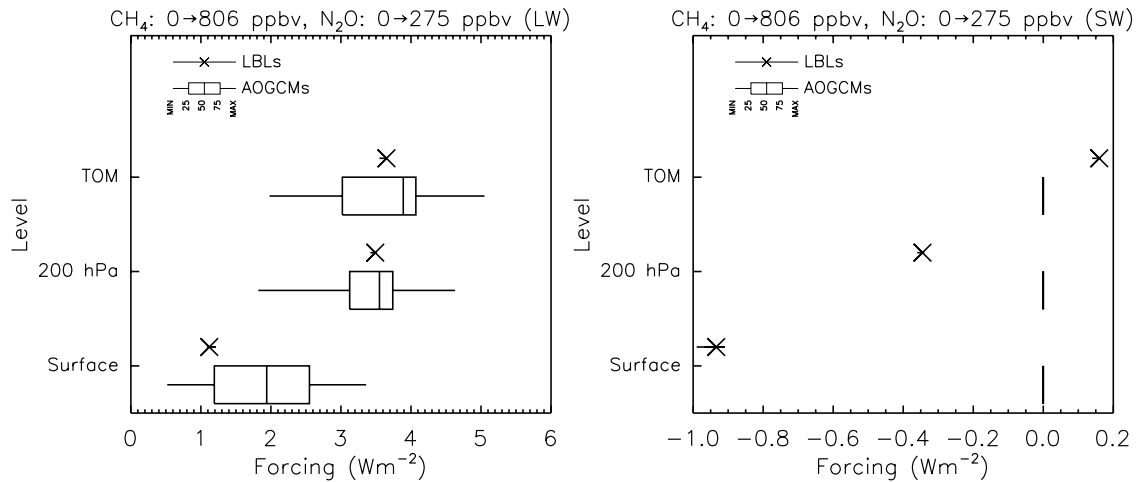


Figure 6. (left) Longwave forcings at TOM, 200 hPa, and the surface for increasing CH₄ from 0 to 806 ppbv and N₂O from 0 to 275 ppbv (case 3a-1a, Table 2; same symbols as Figure 3). (right) Corresponding shortwave forcings.

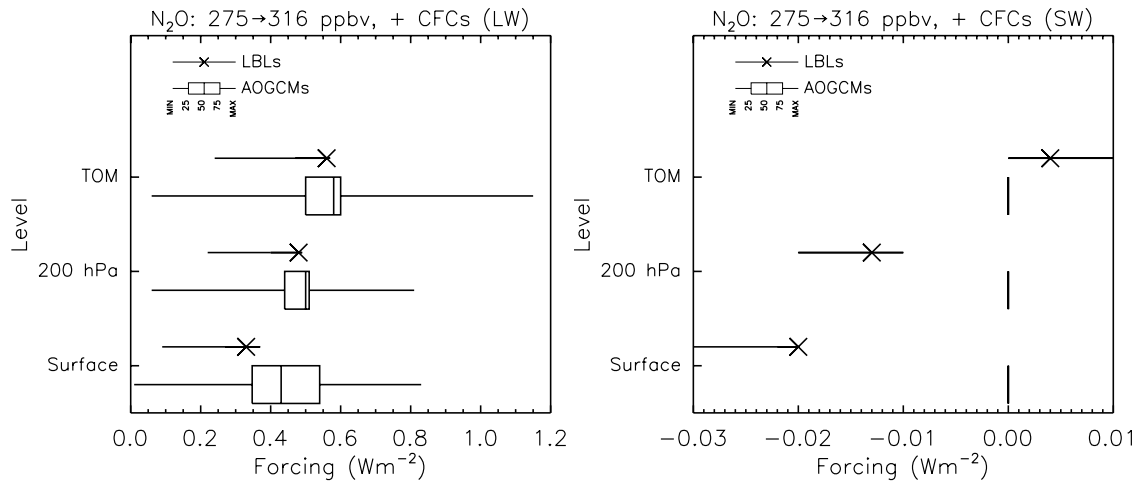


Figure 7. (left) Longwave forcings at TOM, 200 hPa, and the surface for increasing N₂O from 275 to 316 ppbv and CFCs from 0 to year 2000 concentrations (case 3b-3c, Table 2; same symbols as Figure 3).(right) Corresponding shortwave forcings.

atmospheric composition, e.g., increases in WMGHGs. In the RTMIP calculations, the changes in tropospheric flux convergence are smaller in magnitude than 12 W m⁻². From equation 2 it follows that the expected perturbations to $|\bar{Q}|$ are less than approximately 0.1 K/day. For comparison, the global mean shortwave convergence of roughly 67 W m⁻² corresponds to a column-integrated heating of 0.56 K/day, and the global mean longwave convergence of -169 W m⁻² corresponds to a cooling of -1.4 K/day [Kiehl and Trenberth, 1997].

[29] The perturbations to the heating rates for selected forcing cases are shown in Figures 10–13. The cases are doubling CO₂ from concentrations in 1860 (case 2b-1a); increasing CH₄ and N₂O from 0 to values in 1860 (case 3a-1a); increasing the WMGHGs from concentrations in 1860 to 2000 (case 3b-3a); and increasing H₂O by 20% (case 4a-2b). The addition of WMGHGs generally increases the absorption of upwelling longwave and downwelling solar radiation and therefore increases the

corresponding heating rates (Figures 10–12). The addition of H₂O, however, increases the atmospheric emission to the surface by an amount sufficient to cause the atmosphere to cool further (Figure 13, left).

[30] There are three significant features in the comparison of AOGCM and LBL heating rates. First, it is evident from inspection of Figures 10–13 that the differences among the AOGCM calculations are frequently as large as the mean perturbations to the heating rates obtained from the LBL codes. In general, the LBL codes agree amongst themselves in the flux convergences and divergences. Second, the omission of CH₄ and N₂O from the AOGCM shortwave parameterizations is reflected in the zero mean perturbation to AOGCM shortwave heating rates plotted in Figure 11 (right). Third, some of the longwave parameterizations in AOGCMs show evidence of poor numerical formulation or implementation. Two of the AOGCMs produce oscillations in the vertical profile of longwave heating rate perturbations which are absent from the corresponding LBL calculations.

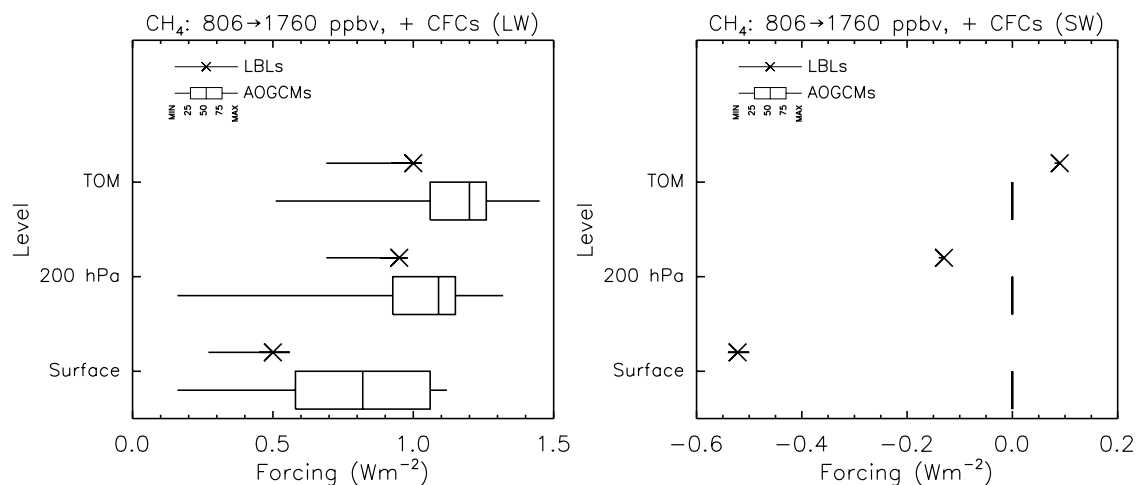


Figure 8. (left) Longwave forcings at TOM, 200 hPa, and the surface for increasing CH₄ from 806 to 1760 ppbv and CFCs from 0 to year 2000 concentrations (case 3b-3d, Table 2; same symbols as Figure 3). (right) Corresponding shortwave forcings.

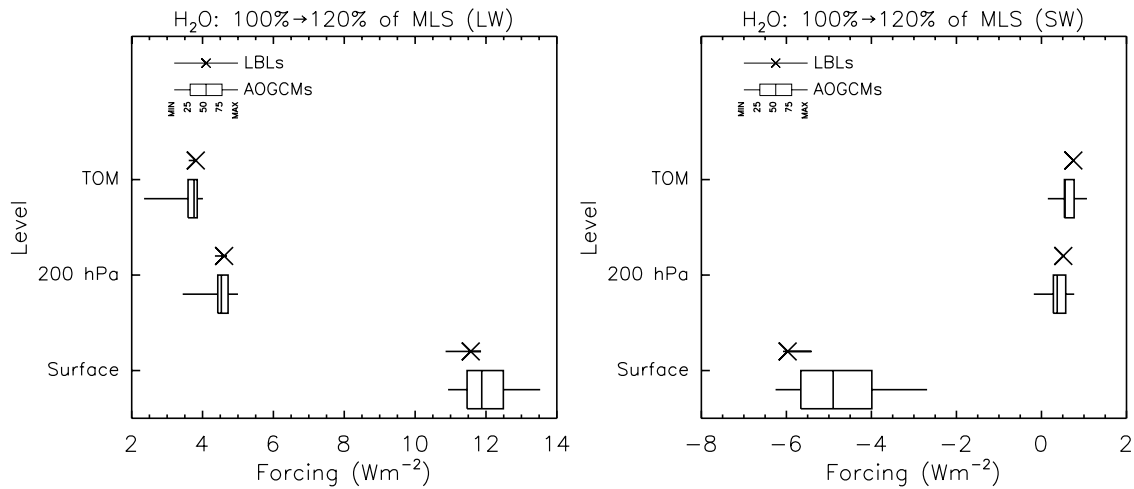


Figure 9. (left) Longwave forcings at TOM, 200 hPa, and the surface for increasing H₂O mixing ratios by 20% through the column (case 4a-2b, Table 2; same symbols as Figure 3). (right) Corresponding shortwave forcings.

These oscillations are particularly evident for the cases of doubling CO₂ (Figure 10, left) and increasing WMGHGs from concentrations in 1860 to 2000 (Figure 12, left). As equation 1 shows, the calculation of heating rates requires numerical differentiation of vertical radiative flux profiles. The existence of these oscillations suggests that some of the AOGCM parameterizations yield flux profiles which are insufficiently continuous with respect to finite differentiation of the vertical coordinate.

4. Discussion and Conclusions

[31] This paper discusses the findings from the Radiative Transfer Model Intercomparison Project (RTMIP). The basic goal of RTMIP is to compare the radiative forcings computed with AOGCMs in the IPCC AR4 against calculations with LBL models. The radiatively active species included in RTMIP are the primary well-mixed greenhouse gases CO₂, CH₄, N₂O, CFC-11, and CFC-12. In the current generation of AOGCMs, the forcings by these species are combined with forcings by a wide variety of other agents

including tropospheric and stratospheric ozone, direct and indirect effects of aerosols, solar variability, land use change, and urbanization [IPCC, 2001]. The participants in RTMIP have focused on WMGHGs since these collectively represent the most important positive forcing on climate [Boucher and Haywood, 2001] and there are minimal uncertainties in the benchmark LBL calculations. Intercomparisons of forcing by other radiatively active species, for example aerosols, are complicated by significant uncertainties in the representations of aerosol chemical composition and microphysical properties. In some sense, an essential criterion for the realism of simulations of climate change with an AOGCM is the fidelity of its calculation of radiative forcing by WMGHGs.

[32] Another metric of radiative parameterizations not considered in RTMIP is the accuracy of the absolute fluxes. The range of clear-sky shortwave fluxes from the participating AOGCMs is considerably larger than the range of shortwave forcings obtained in this study. The difference between the TOM and surface net shortwave fluxes gives the convergence of shortwave radiation in the atmospheric

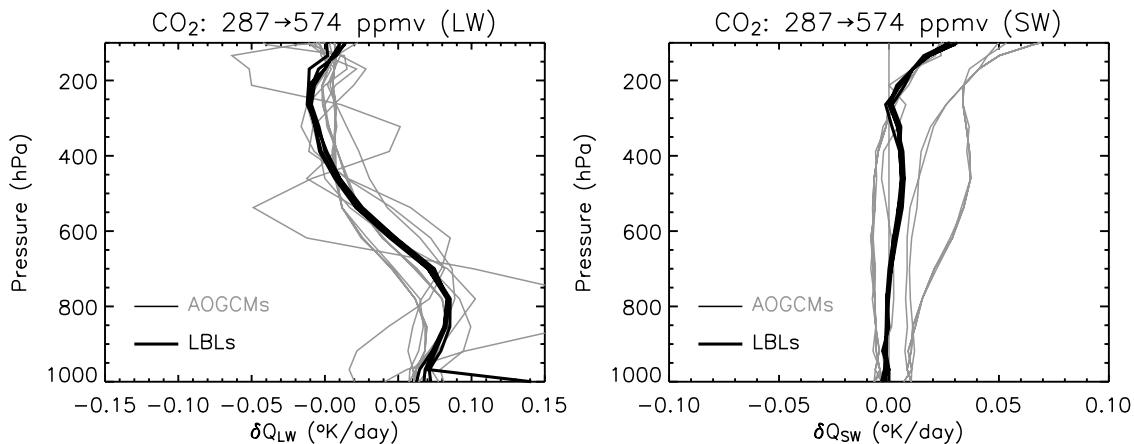


Figure 10. (left) Longwave heating rate perturbations for increasing CO₂ from 287 to 574 ppmv (case 2b-1a, Table 2). (right) Corresponding shortwave heating rate perturbations.

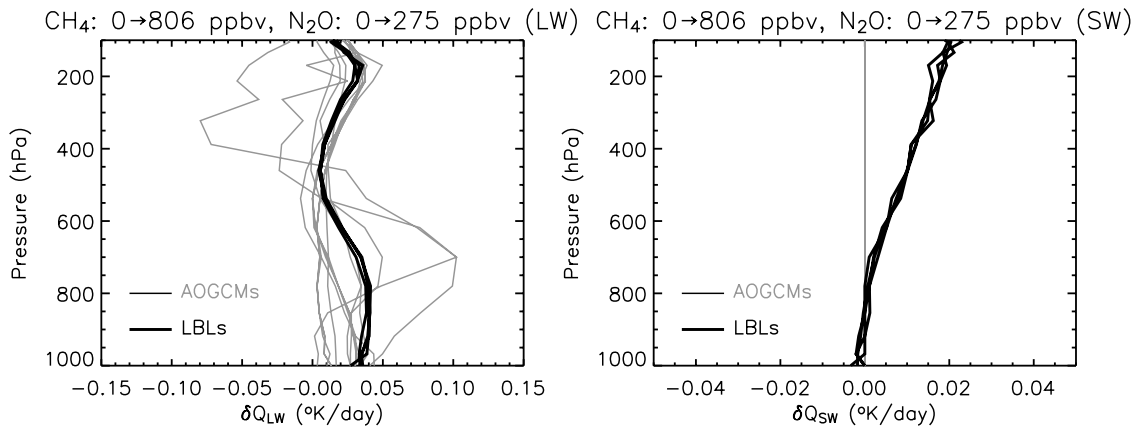


Figure 11. (left) Longwave heating rate perturbations for increasing CH₄ from 0 to 806 ppbv and N₂O from 0 to 275 ppbv (case 3a-1a, Table 2). (right) Corresponding shortwave heating rate perturbations.

column. The clear-sky shortwave convergence has a direct effect on the thermal evolution and the mean atmospheric states simulated with an AOGCM. In the AOGCMs included in RTMIP, the range of clear-sky convergence is approximately 8 W m^{-2} , which is approximately 12% of mean convergence averaged across all models and calculations. The magnitude of the shortwave convergence is governed primarily by the column-integrated masses of absorptive species. Since the masses of the WMGHGs, O₃, and H₂O are identical across the models, the large range of convergence is caused primarily by the diversity of radiative parameterizations across the ensemble of AOGCMs.

[33] Perhaps the most basic finding of RTMIP is that there are no sign errors in the mean forcings averaged across the AOGCM ensemble relative to the LBL calculations. In the set of 672 forcings calculated with individual AOGCMs in RTMIP, there is only one value with an erroneous sign. The average longwave forcings calculated from the AOGCM and LBL codes due to the increase in WMGHGs from 1860 to 2000 differ by less than 0.12 W m^{-2} at the top of model, surface, and pseudotropopause at 200 hPa. The errors in the corresponding mean shortwave forcings are larger, increasing from 0.06 W m^{-2} at TOM to 0.37 W m^{-2} at the surface (a 43% relative error). The biases in short-

wave forcings are caused primarily by the omission of CH₄ and N₂O from the shortwave parameterizations in all of the participating AOGCMs. While the AOGCMs tend to slightly underestimate the longwave forcings by CO₂, the mean shortwave forcings by CO₂ are consistent with the LBL estimates. The mean AOGCM forcings from increased H₂O do not differ significantly from the LBL calculations with the exception of the surface shortwave forcing.

[34] While the mean longwave forcings for the period 1860 to 2000 are in reasonable agreement, the range of longwave forcings at TOM from individual AOGCMs is 1.5 to 2.7 W m^{-2} . This has significant implications for the interpretation of climate change simulations. The global change in surface temperature is linearly related to the total global mean forcing by the climate sensitivity, a measure of the climate feedbacks in a given climate model [IPCC, 2001]. In the absence of adequate information regarding the forcings applied, for example, in multimodel simulations of the 19th and 20th centuries, it is frequently assumed that the forcings by WMGHGs are essentially identical across the ensemble of AOGCMs. If this assumption is valid, then the spread in global mean temperature response across the multimodel ensemble is due to primarily to the spread in the values of climate sensitivity among the

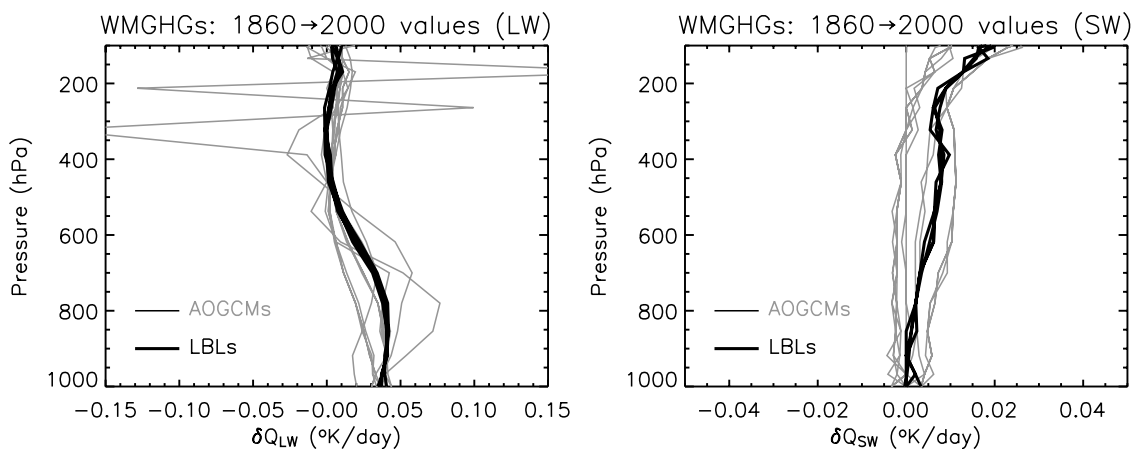


Figure 12. (left) Longwave heating rate perturbations for increasing WMGHGs from year 1860 to year 2000 concentrations (case 3b-3a, Table 2). (right) Corresponding shortwave heating rate perturbations.

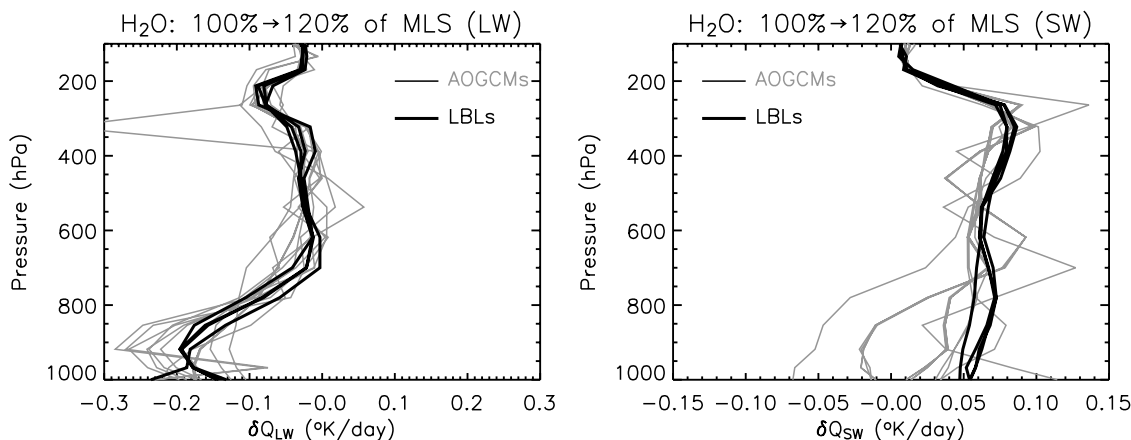


Figure 13. (left) Longwave heating rate perturbations for increasing H_2O mixing ratios by 20% through the column (case 4a-2b, Table 2). (right) Corresponding shortwave heating rate perturbations.

models. However, the results from RTMIP show that this assumption is not tenable for the current generation of AOGCMs. In fact, some of the spread in response should be directly related to the diversity of radiative transfer parameterizations. These findings show that in order to improve the interpretation of climate change simulations from multimodel ensembles, it will be necessary to collect much more complete information on the forcings applied to each of the AOGCMs than has been customary.

[35] The biases in the AOGCM forcings are generally largest at the surface level. For five out of seven surface shortwave forcings and four out of seven surface longwave forcings, differences between the mean AOGCM and LBL calculations are statistically significant. In addition, the largest biases in the shortwave and longwave forcings from all seven experiments occur at the surface layer. The reasonable accuracy of AOGCM forcings at TOM and the significant biases at the surface together imply that the effects of increased WMGHGs on the radiative convergence of the atmosphere are not accurately simulated.

[36] These results suggest several directions for development of the radiative parameterizations in AOGCMs. First, tests of the accuracy of shortwave and longwave forcings at the surface should be given special attention. Second, the shortwave parameterizations in all the AOGCMs should be enhanced to include the effects of CH_4 and optionally N_2O on near-infrared radiation. Third, AOGCMs should evaluate the convergence of shortwave radiation in the atmosphere using benchmark calculations. This is a particularly clean test of the radiation physics, and the current models exhibit an improbably large spread of the convergence. Efforts to address these issues would have several benefits for the climate-modeling community and for groups using their models in scientific and societal applications. Better agreement of AOGCMs with LBL calculations would lead to greater confidence in simulations of past and future climate. It would also facilitate the analysis of forcing response relationships from the complex and heterogeneous multimodel ensembles that have become a standard component of international climate change assessments.

[37] **Acknowledgments.** We acknowledge the international modeling groups for providing their data for analysis, the Program for Climate Model Diagnosis and Intercomparison (PCMDI) for collecting and archiving the

model data, the JSC/CLIVAR Working Group on Coupled Modeling (WGCM) and their Coupled Model Intercomparison Project (CMIP) and Climate Simulation Panel for organizing the model data analysis activity, and the IPCC WG1 TSU for technical and logistical support. The IPCC Data Archive at Lawrence Livermore National Laboratory is supported by the Office of Science in the U.S. Department of Energy. Seung-Ki Min (MIUB) and Asgeir Sorteberg (BCCR) kindly provided special access to their model results. Jeffrey Yin (NCAR) provided critical support by downloading large volumes of model output from the IPCC Data Archive. We would like to thank Petri Raisanen for his comments on the paper and Lawrence Buja (NCAR), Marco Giorgetta (MPI), Andy Lacis (GISS), Seung-Ki Min (MIUB), Erich Roeckner (MPI), Asgeir Sorteberg (BCCR), Bin Wang (LASG), and Joerg Wegner (MPI) for discussions of their AOGCMs. David Edwards (NCAR) and Gene Francis (NCAR) provided very useful assistance and advice regarding their GENLN LBL code. Anu Dudhia (Oxford) provided much assistance in the use of the RFM LBL code. The University of Reading acknowledges support from the Natural Environmental Research Council (via an Advanced Research Fellowship and grant NER/L/S/2001/0066) and the National Physical Laboratory (grant 307981). The efforts of John Yio (LLNL) and Matthew Macduff (PNL) to build the Web-based archive for the RTMIP results have been instrumental in distributing and collecting the data for the intercomparison. Comments by two anonymous reviewers have helped improve the presentation of the results. NCAR is supported by the National Science Foundation.

References

- Anderson, G. P., S. A. Clough, F. X. Kneizys, J. H. Chetwynd, and E. P. Shettle (1986), AFGL atmospheric constituent profiles (0–120 km), *Tech. Rep. AFGL-TR-86-0110*, Air Force Geophys. Lab., Hanscom Air Force Base, Mass.
- Anderson, T. L., R. J. Charlson, S. E. Schwartz, R. Knutti, O. Boucher, H. Rodhe, and J. Heintzenberg (2003), Climate forcing by aerosols—A hazy picture, *Science*, *300*, 1103–1104.
- Barker, H. W., et al. (2003), Assessing 1D atmospheric solar radiative transfer models: Interpretation and handling of unresolved clouds, *J. Clim.*, *16*, 2676–2699.
- Boucher, O., and J. Haywood (2001), On summing the components of radiative forcing of climate change, *Clim. Dyn.*, *18*, 297–302.
- Boucher, O., et al. (1998), Intercomparison of models representing direct shortwave radiative forcing by sulfate aerosols, *J. Geophys. Res.*, *103*, 16,979–16,998.
- Cess, R. D., et al. (1993), Uncertainties in carbon-dioxide radiative forcing in atmospheric general-circulation models, *Science*, *262*, 1252–1255.
- Christidis, N., M. D. Hurlley, S. Pinnock, K. P. Shine, and T. J. Wallington (1997), Radiative forcing of climate change by CFC-11 and possible CFC-replacements, *J. Geophys. Res.*, *102*, 19,597–19,609.
- Clough, A. A., and M. J. Iacono (1995), Line-by-line calculation of atmospheric fluxes and cooling rates: 2. Application to carbon-dioxide, ozone, methane, nitrous-oxide and the halocarbons, *J. Geophys. Res.*, *100*, 16,519–16,535.
- Clough, S. A., F. X. Kneizys, and R. W. Davies (1989), Line shape and the water vapor continuum, *Atmos. Res.*, *23*, 229–241.
- Clough, S. A., M. W. Shephard, E. Mlawer, J. S. Delamere, M. Iacono, K. Cady-Pereira, S. Boukabara, and P. D. Brown (2005), Atmospheric radiative transfer modeling: A summary of the AER codes, *J. Quant. Spectrosc. Radiat. Transfer*, *91*, 233–244.

- Dudhia, A. (1997), RFM v3 software user's manual, *Tech. Rep. ESA PO-MA-OXF-GS-0003*, Atmos., Oceanic, and Planet. Phys., Clarendon Lab., Oxford, U. K.
- Edwards, D. P. (1992), GENLN2: A general line-by-line atmospheric transmittance and radiance model, *Tech. Rep. NCAR/TN-367+STR*, 147 pp., Natl. Cent. for Atmos. Res., Boulder, Colo.
- Ellingson, R. G., and Y. Fouquart (1991), The intercomparison of radiation codes in climate models—An overview, *J. Geophys. Res.*, *96*, 8925–8927.
- Ellingson, R. G., S. J. Ellis, and S. B. Fels (1991), The intercomparison of radiation codes used in climate models—Long-wave results, *J. Geophys. Res.*, *96*, 8929–8953.
- Fels, S. B., J. D. Mahlman, M. D. Schwarzkopf, and R. W. Sinclair (1980), Stratospheric sensitivity to perturbations in ozone and carbon-dioxide—Radiative and dynamical response, *J. Atmos. Sci.*, *37*, 2265–2297.
- Fels, S. B., J. T. Kiehl, A. A. Lacis, and M. D. Schwarzkopf (1991), Infrared cooling rate calculations in operational general circulation models: Comparison with benchmark computations, *J. Geophys. Res.*, *96*, 9105–9120.
- Fouquart, Y., B. Bonnel, and V. Ramaswamy (1991), Intercomparing short-wave radiation codes for climate studies, *J. Geophys. Res.*, *96*, 8955–8968.
- Goody, R. M., and Y. L. Yung, (1989) *Atmospheric Radiation*, 2nd ed., 519 pp., Oxford Univ. Press, New York.
- Halothore, R. N., et al. (2005), Intercomparison of shortwave radiative transfer codes and measurements, *J. Geophys. Res.*, *110*, D11206, doi:10.1029/2004JD005293.
- Hansen, J., M. Sato, and R. Ruedy (1997), Radiative forcing and climate response, *J. Geophys. Res.*, *102*, 6831–6864.
- Intergovernmental Panel on Climate Change (IPCC) (1995), *Climate Change, 1994: Radiative Forcing of Climate Change and an Evaluation of the IPCC IS92 Emission Scenarios*, edited by J. T. Houghton et al., 339 pp., Cambridge Univ. Press, New York.
- Intergovernmental Panel on Climate Change (IPCC) (2001), *Climate Change 2001: The Scientific Basis*, edited by J. T. Houghton et al., 944 pp., Cambridge Univ. Press, New York.
- Kiehl, J. T., and K. E. Trenberth (1997), Earth's annual global mean energy budget, *Bull. Am. Meteorol. Soc.*, *78*, 197–208.
- Kratz, D. P., and F. G. Rose (1999), Accounting for molecular absorption within the spectral range of the CERES window channel, *J. Quant. Spectrosc. Radiat. Transfer*, *61*, 83–95.
- Kratz, D. P., M. G. Mlynczak, C. J. Mertens, H. Brindley, L. L. Gordley, J. Martin-Torres, F. M. Miskolczi, and D. D. Turner (2005), An intercomparison of far-infrared line-by-line radiative transfer models, *J. Quant. Spectrosc. Radiat. Transfer*, *90*, 323–341.
- Labs, D., and H. Neckel (1970), Transformation of the absolute solar radiation data into the “International practical temperature scale of 1968”, *Sol. Phys.*, *15*, 79–87.
- Liou, K.-N., (1992), *Radiation and Cloud Processes in the Atmosphere*, 487 pp., Oxford Univ. Press, New York.
- Manabe, S., and R. T. Wetherald (1975), The effects of doubling the CO₂ concentration on the climate of a general circulation model, *J. Atmos. Sci.*, *37*, 3–15.
- Myhre, G., and F. Stordal (1997), Role of spatial and temporal variations in the computation of radiative forcing and GWP, *J. Geophys. Res.*, *102*, 11,181–11,200.
- Nakicenovic, N., and R. Swart (Eds.) (2000), *Special Report of the Intergovernmental Panel on Climate Change on Emissions Scenarios*, 570 pp., Cambridge Univ. Press, New York.
- Pawson, S., et al. (2000), The GCM-Reality Intercomparison Project for SPARC (GRIPS): Scientific issues and initial results, *Bull. Am. Meteorol. Soc.*, *81*, 781–796.
- Ramanathan, V. (1981), The role of ocean-atmosphere interactions in the CO₂ climate problem, *J. Atmos. Sci.*, *38*, 918–930.
- Ramanathan, V., and R. E. Dickinson (1979), The role of stratospheric ozone in the zonal and seasonal radiative energy balance of the Earth-troposphere system, *J. Atmos. Sci.*, *36*, 1084–1104.
- Ramaswamy, V., and S. M. Freidenreich (1998), A high-spectral resolution study of the near-infrared solar flux disposition in clear and overcast atmospheres, *J. Geophys. Res.*, *103*, 23,255–23,273.
- Randall, D. A., (Ed.) (2000), *General Circulation Model Development*, *Int. Geophys. Ser.*, vol. 70, 807 pp., Elsevier, New York.
- Rothman, L. S., et al. (2003), The HITRAN molecular spectroscopic database: Edition of 2000 including updates of 2001, *J. Quant. Spectrosc. Radiat. Transfer*, *82*, 5–42.
- Schwarzkopf, M. D., and S. B. Fels (1985), Improvements to the algorithm for computing CO₂ transmissivities and cooling rates, *J. Geophys. Res.*, *90*, 10,541–10,550.
- Shine, K. P., B. P. Briegleb, A. S. Grossman, D. Hauglustaine, H. Mao, V. Ramaswamy, M. D. Schwarzkopf, R. van Dorland, and W. C. Wang (1995), Radiative forcing due to changes in ozone: A comparison of different codes, in *Atmospheric Ozone as a Climate Gas: General Circulation Model Simulations*, *NATO ASI Ser., Ser. I*, vol. 32, edited by W. C. Wang and I. S. A. Isaksen, pp. 375–396, Springer, New York.
- Stamnes, K., S. C. Tsay, W. Wiscombe, and K. Jayaweera (1988), A numerically stable algorithm for discrete-ordinate-method radiative transfer in multiple scattering and emitting layered media, *Appl. Opt.*, *27*, 2502–2509.
- Tipping, R. H., and Q. Ma (1995), Theory of the water-vapor continuum and validations, *Atmos. Res.*, *36*, 69–94.
- Tjemkes, S. A., et al. (2003), The ISSWG line-by-line inter-comparison experiment, *J. Quant. Spectrosc. Radiat. Transfer*, *77*, 433–453.
- Trenberth, K. E., (Ed.) (1992), *Climate System Modeling*, 788 pp., Cambridge Univ. Press, New York.
- Tukey, J. W. (1977), Box-and-whisker plots, in *Exploratory Data Analysis*, chap. 2C, pp. 39–43, Addison-Wesley, Reading, Mass.
- Voigt, S., J. Orphal, D. Bogumil, and J. P. Burrows (2001), The temperature dependence (203–293 K) of the absorption cross sections of O₃ in the 230–850 nm region measured by Fourier-transform spectroscopy, *J. Photochem. Photobiol. A*, *143*, 1–9.
- Zhong, W. Y., J. D. Haigh, D. Belmiloud, R. Schermail, and J. Tennyson (2001), The impact of new water vapour spectral line parameters on the calculation of atmospheric absorption, *Q. J. R. Meteorol. Soc.*, *127*, 1615–1626.
- S. E. B. Casanova and L. K. Gohar, Department of Meteorology, University of Reading, Earley Gate, P.O. Box 243, Reading RG6 6BB, UK. (s.e.b.casanova@reading.ac.uk; sws011kg@met.reading.ac.uk)
- W. D. Collins, Climate and Global Dynamics Division, National Center for Atmospheric Research, P.O. Box 3000, Boulder, CO 80307, USA. (wcollins@ucar.edu)
- J.-L. Dufresne and M.-P. Lefebvre, Laboratoire de Météorologie Dynamique (LMD/IPSL), Tour 45–55, 3eme, Jussieu, CNRS/UPMC, Boite 99, F-75252 Paris Cedex 05, France. (jean-louis.dufresne@lmd.jussieu.fr; marie-pierre.lefebvre@lmd.jussieu.fr)
- D. W. Fillmore, LSCE-Orme, Bât. 701, Orme des Merisiers, F-91191 Gif-sur-Yvette, France. (david.fillmore@cea.fr)
- P. M. D. Forster, School of Earth and Environment, University of Leeds, Leeds LS2 9JT, UK. (p.forster@see.leeds.ac.uk)
- Q. Fu, Department of Atmospheric Sciences, University of Washington, 408 ATG Building, P.O. Box 351640, Seattle, WA 98195, USA. (qfu@atmos.washington.edu)
- V. Y. Galin, Institute of Numerical Mathematics, Academy of Sciences, 8 Gubkina Street, Moscow 117333, Russia. (galin@inm.ras.ru)
- W. J. Ingram, Department of Physics, Clarendon Laboratory, Parks Road, Oxford OX1 3PU, UK. (ingram@atm.ox.ac.uk)
- D. P. Kratz, Climate Science Branch, NASA Langley Research Center, MS 420, 21 Langley Boulevard, Hampton, VA 23681, USA. (david.p.kratz@nasa.gov)
- J. Li, Canadian Centre for Climate Modeling and Analysis, University of Victoria, P.O. Box 1700, STN CSC, Victoria, BC, Canada V8W 2Y2. (jiangnan.li@ec.gc.ca)
- P. Marquet, Météo-France, CNRM, 42 avenue G. Coriolis, F-31057 Toulouse Cedex 01, France. (pascal.marquet@meteo.fr)
- V. Oinas, NASA Goddard Institute for Space Studies, 2880 Broadway, New York, NY 10025, USA. (voinas@giss.nasa.gov)
- R. W. Portmann, Aeronomy Laboratory, NOAA, 325 Broadway, Boulder, CO 80305, USA. (robert.w.portmann@noaa.gov)
- V. Ramaswamy and M. D. Schwarzkopf, Geophysical Fluid Dynamics Laboratory, 201 Forrestal Road, Princeton, NJ 08542, USA. (v.ramaswamy@noaa.gov; dan.schwarzkopf@noaa.gov)
- Y. Sun, National Climate Center, CMA, Laboratory for Climate Change, 46 South Zhongguancun Avenue, Beijing 100081, China. (sunying@cma.gov.cn)
- Y. Tsushima, Frontier Research Center for Global Change, Japan Agency for Marine-Earth Science and Technology, 3173-25 Showa-machi, Kanazawa-ku, Yokohama 236-0001, Japan. (tsussi@jamstec.go.jp)
- T. Uchiyama, Meteorological Research Institute, 1-1 Nagamine, Tsukuba-shi, Ibaraki-ken 305-0052, Japan. (tuchiyam@mri-jma.go.jp)
- W. Y. Zhong, Space and Atmospheric Physics Group, Physics Department, Imperial College, Prince Consort Road, London SW7 2BW, UK. (w.zhong@imperial.ac.uk)